Statistical properties of speckle patterns for a random number of scatterers and nonuniform phase distributions

Fernando L. Metz, Cristian Bonatto, and Sandra D. Prado
Physics Institute, Federal University of Rio Grande do Sul, 91501-970 Porto Alegre, Rio Grande do Sul, Brazil

(Received 18 September 2023; accepted 12 December 2023; published 2 January 2024)

The statistical properties of speckle patterns have important applications in optics, oceanography, and transport phenomena in disordered systems. Here we obtain closed-form analytic results for the amplitude distribution of speckle patterns formed by a random number of partial waves characterized by an arbitrary phase distribution, generalizing classical results of the random-walk theory of speckle patterns. We show that the functional form of the amplitude distribution is solely determined by the distribution of the number of scatterers, while the phase distribution only influences the scale parameters. In the case of a nonrandom number of scatterers, we find an analytic expression for the amplitude distribution that extends the Rayleigh law to nonuniform random phases. For a negative binomial distribution of the number of scatterers, our results reveal that large fluctuations of the wave amplitudes become more pronounced in the case of biased random phases. We present numerical results that fully support our analytic findings.

DOI: 10.1103/PhysRevA.109.013501

I. INTRODUCTION

Waves propagating in random media undergo multiple scattering from inhomogeneities [1]. The scattered waves interfere with each other and give rise to an irregular intensity pattern that echoes the random structure of the sample. In optics, the most straightforward realization of this basic phenomenology occurs when a laser beam is reflected by a rough surface, leading to the formation of a granular intensity pattern known as a speckle pattern [2–4]. Studies of various aspects linked to speckle formation have been carried out since the invention of lasers, which remain an active area of research [4,5]. Prominent statistical properties include not only the intensity distribution but also other speckle distributions, such as those related to light polarization [6] and phase singularities [7]. Another important topic that has been experiencing rapid development from both a theoretical and an experimental point of view is the study of three-dimensional speckle patterns [8–10]. The statistical properties of speckle patterns find important applications in hydrodynamics [11], medical science [12], imaging techniques [13–15], material science [16,17], multimode fiber systems [18], optical radar performance [19], and transport phenomena in disordered systems [20,21].

The random-walk model is the simplest theoretical approach to study speckle patterns [2,3]. In this framework, the resultant electromagnetic field observed at a specific point is the superposition of a large number of partial waves, each one arising from an individual scatterer within the sample. Each contribution to the speckle field carries a random phase, whose statistical properties reflect the spatial arrangement of the scatterers. The problem is formally equivalent to a random walk in two dimensions [3,22]. When the phases are independent random variables, the central-limit theorem holds and the resultant electromagnetic field follows a Gaussian distribution. In the strong-scattering regime, where the phases are uniformly distributed, the amplitude of the resultant field follows the well-known Rayleigh distribution [2,3]. In the weak-scattering regime, in which the phases exhibit weak fluctuations around a constant value, the amplitude obeys the Rice distribution [3].

The breakdown of the central-limit theorem in the random-walk model leads to deviations from both the Rayleigh and the Rice distribution. Indeed, non-Rayleigh statistics emerges in the strong-scattering regime as long as the phases are correlated random variables [23–27] or the number of scatterers is finite [28–30]. More fundamental approaches, based on the solutions of the classical wave equation [20,31], have shown that the exponential tail of the Rayleigh distribution fails to reproduce the statistics of large amplitudes [20,32,33]. In the context of random-walk models, Jakeman and Pusey [34] put forward a phenomenological model for the strong-scattering regime in which the number of scatterers is itself a random variable. When the variance of the number of scatterers is large enough, the amplitude of the resultant speckle field follows the so-called K distribution, which has been recognized as a very good model for scattering experiments involving turbulent media [35,36]. From a more theoretical perspective, the K distribution can be seen as a consequence of the breakdown of the central-limit theorem, which occurs due to the fluctuating number of scatterers [22,34,36,37].

Theoretical approaches for speckle patterns have traditionally focused on the limiting cases of strong- and weak-scattering regimes. The Rayleigh distribution characterizes amplitude fluctuations resulting from a highly inhomogeneous medium, while the Rice distribution arises from a quasihomogeneous medium. In these two limits, the phases of the partial waves are uniformly distributed. On the other hand, much less attention has been devoted to the scattering of waves with nonuniform phase distributions, i.e., physical situations

in which the values of the phases have different statistical weights. These cases are of physical relevance since nonuniform phase distributions play an important role in a number of practical situations, such as the scattering from a finite disordered sample [38], the speckle patterns formed in the near-field region [39–41], and the amplitude fluctuations arising from nonisotropic arrangements of scatterers [42].

Concerning nonuniform random phases, there have been a few attempts [22,36,43] to generalize the random-walk model of speckle patterns to include this feature. Barakat [43] derived the amplitude distribution in the particular case of a von Mises phase distribution, while Jakeman and Tough [22,36] considered a weak perturbation around the uniform phase distribution. Despite the fact that many results from the classical speckle theory have been developed a long time ago, the interest in the statistical properties of both linear and nonlinear wave propagation has been renewed with the growing interest in extreme wave generation [26,44–47]. However, a systematic approach to calculate the amplitude distribution of speckle patterns for a generic distribution of phases is lacking. The purpose of our paper is to fill this gap.

Here we introduce an exactly solvable random-walk model for speckle patterns generated by a random number of scatterers with an arbitrary phase distribution. By distinguishing between biased and unbiased random phases, we derive general analytic expressions for the amplitude distribution of the speckle field, from which one can find several closed-form analytic results that cover a rich variety of specific situations, generalizing classical results [2,34] within the theory of speckle patterns. In particular, we find an analytic result for the amplitude distribution in the simple case of a nonrandom number of scatterers, which extends the Rayleigh law to arbitrary phase distributions. We show that the distribution of the number of scatterers fully determines the functional form of the amplitude distribution, while the information about the phase distribution is encoded in the scale parameters characterizing the joint distribution of the speckle field. For a negative binomial distribution of the number of scatterers, we show that amplitude fluctuations become more pronounced in the case of biased random phases, due to a power-law tail in the amplitude distribution. The exactness of our theoretical findings are fully confirmed by numerical simulations.

The paper is organized as follows. In the next section we introduce the random-walk model for the scattering by an inhomogeneous surface with a random number of scatterers. Section III presents the main analytic results for the amplitude distribution in the cases of biased and unbiased random phases. In Sec. IV we summarize our results and discuss some prospects for future work. Appendix A explains all details involved in the derivation of the main analytic findings of Sec. III, while in Appendix B we demonstrate a useful identity to obtain closed-form expressions for the amplitude distribution when the number of scatterers follows a negative binomial distribution.

II. RANDOM-WALK MODEL FOR SPECKLE PATTERNS

In this work we focus on the random-walk model of speckle patterns. One of the original motivations for introducing this phenomenological model is the study of the interference pattern formed at a large distance from an irregular surface [2,3,36]. For concreteness, we consider a one-dimensional regular lattice of length L with N sites or positions labeled by $j = 0, \ldots, N-1$, in which the distance between two adjacent sites is given by $\frac{L}{N-1}$. Each site is occupied by a pointlike source that emits coherent light with wavelength λ. We study the distribution of the amplitude that characterizes the resulting interference pattern emerging at a large distance from the sample (Fraunhofer diffraction). Since pointlike scatterers emit spherically symmetric partial waves, we assume that the amplitudes of all individual waves are equal to a constant E_0. Let ϕ_j $(j = 0, \ldots, N-1)$ be the phase of the partial wave arising from the j scatterer. The electromagnetic field on a screen or observation plane located at a large distance from the sample is given by

$$E(\beta) = E_0 \sum_{j=0}^{N-1} e^{ij[\beta/(N-1)]+i\phi_j}, \tag{1}$$

where

$$\beta = 2\pi \frac{L}{\lambda} \sin(\theta) \tag{2}$$

is given in terms of the angular position $\theta \in (-\frac{\pi}{2}, \frac{\pi}{2})$ on the screen.

Equation (1) holds when all partial waves arrive on the screen. There are different reasons to drop this assumption and consider a more realistic scenario in which light is emitted only by a fraction of scatterers randomly placed over the sample. This class of models is particularly relevant when the scatterers exhibit dynamic behavior, moving in and out of the illuminated region due to dynamical processes [37]. A minimal microscopic model of this situation is represented by the expression for the electric field

$$E(\beta) = E_0 \sum_{j=0}^{N-1} x_j e^{ij[\beta/(N-1)]+i\phi_j}, \tag{3}$$

where the binary random variable $x_j \in \{0, 1\}$ tells whether the individual wave labeled by j reaches the detector. If $x_j = 1$, then the j wavefront reaches the screen; otherwise $x_j = 0$. Therefore, the occupation random variables $x_0, \ldots, x_{N-1}$ determine the (random) positions of the scatterers along the one-dimensional lattice. The total number $k = 0, \ldots, N-1$ of wavefronts that reach the screen is now given by

$$k = \sum_{j=0}^{N-1} x_j. \tag{4}$$

Note that the speckle field in Eq. (3) is a sum of k terms. The phases $\phi_0, \ldots, \phi_{N-1}$ are independent random variables that follow an arbitrary distribution $\Omega(\phi)$.

In order to complete the definition of the model, we need to specify the distribution of $x_0, \ldots, x_{N-1}$. The discrete quantity $k = 0, \ldots, N-1$ is itself a random variable that models the microscopic fluctuations of the number of scatterers among different samples. Given a certain value of k, we choose the

conditional joint distribution $P(\boldsymbol{x}|k)$ of $\boldsymbol{x} = (x_0, \ldots, x_{N-1})$ as

$$P(\boldsymbol{x}|k) = \frac{1}{\mathcal{N}_k}\delta_{k,\sum_{j=0}^{N-1} x_j} \times \prod_{j=0}^{N-1}\left[\frac{k}{N}\delta_{x_j,1} + \left(1-\frac{k}{N}\right)\delta_{x_j,0}\right], \tag{5}$$

where $\mathcal{N}_k$ is the normalization factor for finite N. In the limit $N \to \infty$, this factor converges to $\mathcal{N}_k^{(\infty)} = \frac{e^{-k}k^k}{k!}$. According to Eq. (5), the variables $x_0, \ldots, x_{N-1}$ are independently drawn from a bimodal distribution, where $x_j = 1$ with probability k/N and $x_j = 0$ with probability $1 - k/N$. The term containing the Kronecker δ ensures that the constraint $k = \sum_{j=0}^{N-1} x_j$ is fulfilled for each realization of the model. The object $P(\boldsymbol{x}|k)$ is the conditional probability for a fixed k, while the joint distribution $p(\boldsymbol{x})$ is obtained from

$$p(\boldsymbol{x}) = \sum_{k=0}^{N} p_k P(\boldsymbol{x}|k), \tag{6}$$

where p_k is the discrete probability of k. Equations (5) and (6) completely define the distribution of $x_0, \ldots, x_{N-1}$.

Our primary aim is to compute the probability distribution $\mathcal{P}_\beta(A)$ of the amplitude

$$A(\beta) = |E(\beta)|, \tag{7}$$

generalizing classical results [2,34] of the theory of speckle patterns to arbitrary phase distributions $\Omega(\phi)$. Once the analytic form of $\mathcal{P}_\beta(A)$ is known, the distribution $\mathcal{F}_\beta(I)$ of the intensity $I = A^2$ is determined by the relation $\mathcal{F}_\beta(I) = (4I)^{-1/2}\mathcal{P}_\beta(\sqrt{I})$, which is obtained by a simple change of variables. Since N is the number of available positions of the scatterers along the sample, the average density of scatterers is given by

$$D = \frac{a}{N}, \tag{8}$$

where a is the average number of scatterers

$$a = \sum_{k=0}^{N} p_k k. \tag{9}$$

In the next section we present analytic expressions for $\mathcal{P}_\beta(A)$ in the regime where both N and a are infinitely large but the density D goes to zero. This low-density regime is achieved by setting $a \propto N^\delta$ ($\delta < 1$) and then taking the limit $N \to \infty$. Put differently, our analytic findings are valid in the regime where the average number of scatterers is very large but much smaller than the total number of available spaces in the sample.

III. DISTRIBUTION OF AMPLITUDES

In this section we present the main analytic results for $\mathcal{P}_\beta(A)$. Let $\mathcal{W}_\beta(E_R, E_I)$ be the joint probability distribution of the complex field $E(\beta) = E_R(\beta) + iE_I(\beta)$ for fixed β. In order to obtain a finite limit of $\mathcal{W}_\beta(E_R, E_I)$ as $a \to \infty$, we need to rescale the amplitude E_0 with respect to a. The rescaling factor depends on the choice of the distribution $\Omega(\phi)$ of phases $\phi_0, \ldots, \phi_{N-1}$. Thus, although there is no need to fully specify the form of $\Omega(\phi)$ to derive the expressions for $\mathcal{P}_\beta(A)$, we do have to distinguish between two different families of distributions, since E_0 has to be rescaled differently in each case. Let $\langle f(\phi)\rangle_\phi$ be the average of a function $f(\phi)$ of the random phase ϕ,

$$\langle f(\phi)\rangle_\phi = \int_0^{2\pi} d\phi\, \Omega(\phi) f(\phi). \tag{10}$$

For unbiased random phases, $\Omega(\phi)$ is such that $\langle e^{i\phi}\rangle_\phi = 0$ and we rescale the amplitude of the speckle field as $E_0 \to E_0/\sqrt{a}$. An important example of an unbiased distribution $\Omega(\phi)$ is the uniform distribution in the interval $[0, 2\pi)$, which characterizes the strong-scattering regime. For biased random phases, $\Omega(\phi)$ is such that $\langle e^{i\phi}\rangle_\phi \neq 0$ and the amplitude must be rescaled as $E_0 \to E_0/a$. The most straightforward example of biased phases arises when all phases are set to a constant value.

Apart from the aforementioned constraints on $\Omega(\phi)$, our main analytic results hold for arbitrary distributions p_k and $\Omega(\phi)$. In other words, both the distribution of the number of scatterers and the phase distribution are inputs of the analytic expressions. Nevertheless, for the purpose of generating numerical results, we do have to specify p_k and $\Omega(\phi)$. As a simple example of a nonuniform $\Omega(\phi)$, we will consider a bimodal distribution

$$\Omega(\phi) = q\delta(\phi - \phi_0) + (1-q)\delta(\phi - \phi_0 - \pi), \tag{11}$$

where $\phi_0 \in [0, 2\pi)$ and $q \in [0, 1]$. According to Eq. (11), we randomly select phases ϕ_0 and $\phi_0 + \pi$ with probabilities q and $1 - q$, respectively. When $q = \frac{1}{2}$, Eq. (11) produces an unbiased distribution, while for $q \neq \frac{1}{2}$, the distribution $\Omega(\phi)$ becomes biased.

As we will see below, when a approaches infinity, the statistics of the number of scatterers is encoded in the function

$$\nu(g) = \lim_{a\to\infty} \sum_{k=0}^{N} p_k \delta\left(g - \frac{k}{a}\right), \tag{12}$$

which provides the distribution of the rescaled number k/a of scatterers when $a \to \infty$. The shape of $\nu(g)$ is dictated by the discrete distribution p_k. When discussing explicit results for the amplitude distribution, it is convenient to distinguish between two regimes that characterize the fluctuations of the number k of scatterers. Let Δ_ν^2 be the variance of $\nu(g)$. In the regime of weak fluctuations of k, the discrete distribution p_k is such that $\nu(g) = \delta(g-1)$ and therefore $\Delta_\nu = 0$. A typical example where p_k results in vanishing fluctuations in the number of scatterers is given by the Poisson distribution $p_k = \frac{a^k e^{-a}}{k!}$. In the regime of strong fluctuations of k, p_k is such that $\nu(g)$ has a finite variance ($\Delta_\nu > 0$).

We model the regime of strong fluctuations by following [34] and considering a negative binomial distribution of the number of scatterers

$$p_k = \frac{\Gamma(\mu+k)}{\Gamma(\mu)}\frac{1}{k!}\left(\frac{a}{\mu}\right)^k \frac{1}{(1+a/\mu)^{\mu+k}}, \tag{13}$$

where the parameter $\mu > 0$ controls the variance σ_k^2 of p_k according to

$$\sigma_k^2 = a + \frac{a^2}{\mu}. \tag{14}$$

As $\mu \to \infty$, Eq. (13) converges to a Poisson distribution with mean a and we recover the regime of weak fluctuations. For $\mu = 1$, Eq. (13) gives rise to the geometric (or exponential) distribution

$$p_k = \frac{1}{a+1}\left(\frac{a}{a+1}\right)^k. \tag{15}$$

From a practical perspective, the negative binomial distribution can be interesting to study the scattering by samples in which spatial correlations in the positions of the scatterers induce the formation of clusters of fluctuating size. If the size L of the scattering region is comparable to the correlation length, the number of scatterers inside the region defined by L should display large fluctuations. This argument has motivated the use of the negative binomial distribution in random-walk models that fit empirical data obtained from scattering experiments with a variety of turbulent systems [34,36].

Inserting Eq. (13) into Eq. (12), one can show that the corresponding $\nu(g)$ is the Γ distribution

$$\nu(g) = \frac{\mu^\mu}{\Gamma(\mu)} g^{\mu-1} e^{-\mu g}, \tag{16}$$

whose variance is given by

$$\Delta_\nu^2 = \frac{1}{\mu}. \tag{17}$$

The above equation further clarifies why this model is interesting. The Γ distribution (16) interpolates between the regimes of weak fluctuations ($\mu \to \infty$) and strong fluctuations ($\mu \to 0$) by only changing a single parameter μ. As expected, Eq. (16) reduces to the exponential distribution $\nu(g) = e^{-g}$ for $\mu = 1$.

In summary, the distribution $\nu(g)$, analogous to the continuous version of p_k, along with $\Omega(\phi)$, determines the shape of the amplitude distribution $\mathcal{P}_\beta(A)$. In the following sections we discuss explicit results where $\Omega(\phi)$ and $\nu(g)$ follow Eqs. (11) and (16), respectively.

A. Biased phases

First, we present the analytic results for distributions of phases that fulfill $\langle e^{i\phi}\rangle_\phi \neq 0$. In this case, the joint distribution $\mathcal{W}_\beta(E_R, E_I)$ of the complex field $E(\beta) = E_R(\beta) + iE_I(\beta)$ [Eq. (3)] is given by

$$\mathcal{W}_\beta(E_R, E_I) = \int_0^\infty dg\, \nu(g)\delta(E_R - g\,\mathrm{Re}E_*(\beta)) \times \delta(E_I - g\,\mathrm{Im}E_*(\beta)), \tag{18}$$

where the mean value $E_*(\beta)$ of the speckle field is a function of the position β on the screen, namely,

$$E_*(\beta) = \frac{E_0}{\beta}\langle \sin(\beta+\phi) - \sin\phi\rangle_\phi + i\frac{E_0}{\beta}\langle \cos\phi - \cos(\beta+\phi)\rangle_\phi. \tag{19}$$

Equation (18) is valid when both N and a become infinitely large, but the average density $D = a/N$ of the number of scatterers goes to zero.

The distribution $\mathcal{P}_\beta(A)$ of the amplitude readily follows from Eqs. (7) and (18),

$$\mathcal{P}_\beta(A) = \frac{1}{|E_*(\beta)|}\nu\left(\frac{A}{|E_*(\beta)|}\right). \tag{20}$$

The above result holds for any distribution $\Omega(\phi)$ of phases, provided $\langle e^{i\phi}\rangle_\phi \neq 0$, and for any distribution $\nu(g)$ of the rescaled number of scatterers. The distribution $\nu(g)$ controls the functional form of $\mathcal{P}_\beta(A)$, while $\Omega(\phi)$ appears in the scale parameter $|E_*(\beta)|$. We explain how to derive Eqs. (19) and (20) in Appendix A.

The moments of the amplitude are directly obtained from the moments of $\nu(g)$. By defining $\langle A^n\rangle$ as the nth moment of $\mathcal{P}_\beta(A)$, it is straightforward to show that the first and second moments of the amplitude are given by

$$\langle A\rangle = |E_*(\beta)| \tag{21}$$

and

$$\langle A^2\rangle = |E_*(\beta)|^2\left(1 + \Delta_\nu^2\right), \tag{22}$$

respectively. Hence, the contrast of the speckle pattern, which is the relative standard deviation of A, is solely determined by the standard deviation Δ_ν of the number of scatterers in the medium, i.e.,

$$\frac{\sqrt{\langle A^2\rangle - \langle A\rangle^2}}{\langle A\rangle} = \Delta_\nu. \tag{23}$$

Clearly, strong fluctuations in the number of scatterers lead to pronounced fluctuations in the intensity across the screen. Equations (20) and (23) hold for an arbitrary distribution $\nu(g)$.

In the regime of weak fluctuations in the number of scatterers, we have that $\nu(g) = \delta(g-1)$, and Eq. (20) leads to

$$\mathcal{P}_\beta(A) = \delta(A - |E_*(\beta)|). \tag{24}$$

Hence, if the tail of p_k decays sufficiently fast, the distribution of the amplitude becomes peaked at its average value $|E_*(\beta)|$. Using the explicit form of $E_*(\beta)$ [Eq. (19)], we can rewrite $\mathcal{P}_\beta(A)$ as

$$\mathcal{P}_\beta(A) = \delta\left(A - \sqrt{\langle\sin\phi\rangle_\phi^2 + \langle\cos\phi\rangle_\phi^2}\,\frac{2E_0}{\beta}\sin\left(\frac{\beta}{2}\right)\right). \tag{25}$$

This is the sinc function multiplied by a factor that depends on the phase distribution. Thus, for biased distributions $\Omega(\phi)$, despite phases being generally random variables, the amplitude equals its average value as long as $\Delta_\nu = 0$. Figure 1 shows numerical histograms of the amplitude obtained from Eq. (3) for different sizes N in the regime of weak fluctuations in the number of scatterers. Clearly, as N increases, the histograms in (3) become sharply peaked at $\langle A\rangle = |E_*(\beta)|$, confirming Eq. (25). When all phases are equal to a constant, Eq. (25) reduces to the usual sinc function.

In the regime of strong fluctuations in the number of scatterers, we combine Eqs. (16) and (20) and obtain the explicit formula

$$\mathcal{P}_\beta(A) = \frac{\mu^\mu}{|E_*(\beta)|^\mu\Gamma(\mu)} A^{\mu-1} e^{-\mu A/|E_*(\beta)|}. \tag{26}$$

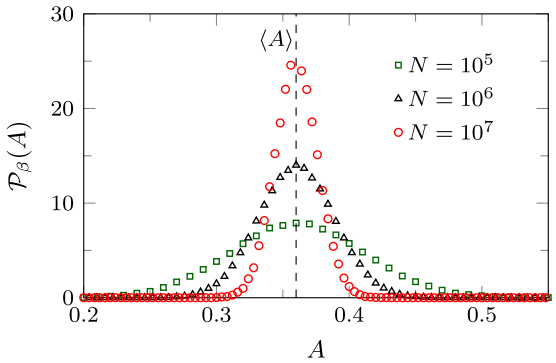

FIG. 1. Numerical results for the distribution of the amplitude for $\beta = \pi/2$ in the regime of weak fluctuations in the number of scatterers. The biased random phases are drawn from the bimodal distribution of Eq. (11), with $q = 0.7$ and $\phi_0 = \pi/4$, while the number of scatterers k follows a Poisson distribution with average $a = \sqrt{N}$. The numerical results are generated from 10^5 realizations of Eq. (3) with different N. The dashed vertical line marks the average amplitude $\langle A\rangle = |E_*(\beta)|$ for $N \to \infty$ [see Eq. (24)]

Figure 2 compares Eq. (26) with histograms of the amplitude generated from numerical results for finite N. The latter are obtained from Eq. (3) for several realizations of the model. Figure 2 demonstrates the exactness of Eq. (26) in depicting the amplitude distribution in cases involving biased random phases and strong fluctuations in the number of scatterers.

Equation (26) reveals two interesting consequences of the strong fluctuations in the number of scatterers. The first one concerns the dramatic change in $\mathcal{P}_\beta(A \to 0)$ as a function of the variance $\Delta_\nu^2 = 1/\mu$. For $\mu > 1$, we obtain $\lim_{A\to 0}\mathcal{P}_\beta(A) = 0$, while the amplitude distribution diverges as a power law $\mathcal{P}_\beta(A) \propto A^{\mu-1}$ $(A \to 0)$ for $\mu < 1$. For $\mu = 1$, $\lim_{A\to 0}\mathcal{P}_\beta(A)$ converges to a finite value. The second interesting feature concerns the behavior of $\mathcal{P}_\beta(A)$ for large amplitudes, as illustrated in Fig. 3. For large A, $\mathcal{P}_\beta(A)$ exhibits a power-law tail $A^{\mu-1}$ $(\mu < 1)$ that extends up to a threshold

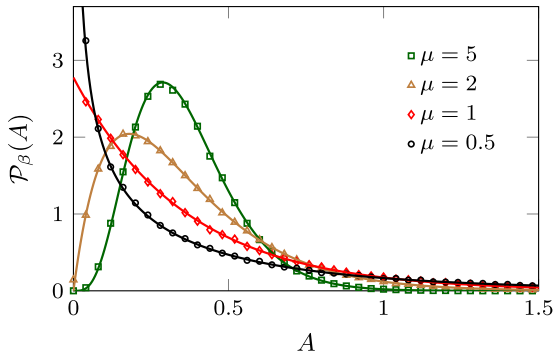

FIG. 2. Comparison between the analytic expression for the distribution of the amplitude [Eq. (26)] (solid lines) and numerical results (symbols) for $\beta = \pi/2$ and biased random phases. The rescaled number of scatterers $\nu(g)$ follows a Γ distribution with variance $1/\mu$ [see Eq. (16)]. The phases are drawn from the bimodal distribution of Eq. (11), with $q = 0.7$ and $\phi_0 = \pi/4$. The numerical results (different symbols) are obtained from 2×10^5 realizations of the model with $N = 10^7$, where the number of scatterers is drawn from a negative binomial distribution with mean $a = \sqrt{N}$ [see Eq. (13)].

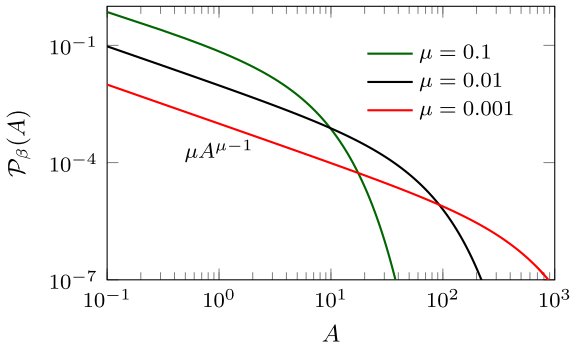

FIG. 3. Tails of the distribution of the amplitude for biased random phases and $\beta = \pi/2$. These results, obtained from Eq. (26), are shown in logarithmic scale. The rescaled number of scatterers follows a Γ distribution $\nu(g)$ with variance $1/\mu$ [see Eq. (16)]. The phases are drawn from the bimodal distribution of Eq. (11), with $q = 0.7$ and $\phi_0 = \pi/4$.

of $O(|E_*(\beta)|/\mu)$. For $A \gtrsim |E_*(\beta)|/\mu$, the exponential factor in Eq. (26) becomes important and suppresses the power-law decay. The value of the threshold that separates the power-law and exponential regimes diverges as $\mu \to 0$, which highlights the appearance of huge fluctuations in the amplitude. In summary, for $\mu < 1$, although the probability to observe a vanishing amplitude at a given point β on the screen is very large, there is a significant probability to observe an extremely large amplitude in comparison to $\langle A\rangle$. The occurrence of such rare events is enhanced by increasing the fluctuations in the number of scatterers.

B. Unbiased phases

Here we present the analytic results for phase distributions $\Omega(\phi)$ that satisfy the constraint $\langle e^{i\phi}\rangle_\phi = 0$. In this case, the distribution of the complex field $E(\beta) = E_R(\beta) + iE_I(\beta)$ reads

$$\mathcal{W}_\beta(E_R, E_I) = \frac{1}{2\pi E_0^2 \sigma_R \sigma_I \sqrt{1-\rho^2}} \int_0^\infty \frac{dg\,\nu(g)}{g} \times \exp\left[-\frac{1}{2gE_0^2(1-\rho^2)} \times\left(\frac{E_R^2}{\sigma_R^2} + \frac{E_I^2}{\sigma_I^2} - \frac{2\rho}{\sigma_R\sigma_I}E_R E_I\right)\right], \tag{27}$$

where σ_R, σ_I, and ρ are given by

$$\sigma_R^2 = \frac{1}{2} + \frac{1}{4\beta}\langle \sin(2\beta + 2\phi) - \sin(2\phi)\rangle_\phi, \tag{28}$$

$$\sigma_I^2 = \frac{1}{2} - \frac{1}{4\beta}\langle \sin(2\beta + 2\phi) - \sin(2\phi)\rangle_\phi, \tag{29}$$

$$\rho = \frac{1}{4\beta\sigma_R\sigma_I}\langle \cos(2\phi) - \cos(2\beta + 2\phi)\rangle_\phi. \tag{30}$$

The above parameters thus depend on the phase distribution $\Omega(\phi)$ as well as on the position β along the screen. In the regime of weak fluctuations in the number of scatterers ($\Delta_\nu = 0$), Eq. (27) reduces to a bivariate Gaussian distribution, which is a direct consequence of the central-limit theorem as applied

to a random walk in two dimensions [2]. In the regime of strong fluctuations in the number of scatterers ($\Delta_\nu > 0$), the central-limit theorem breaks down and one has to specify $\nu(g)$ to determine $\mathcal{W}_\beta(E_R, E_I)$.

Equation (27) yields the analytic expression for the distribution of the amplitude

$$\mathcal{P}_\beta(A) = \int_0^\infty \frac{dg\,\nu(g)}{g} \mathcal{C}_\beta(A|g), \tag{31}$$

where

$$\mathcal{C}_\beta(A|g) = \frac{A}{E_0^2\sigma_R\sigma_I\sqrt{1-\rho^2}} \exp\left(-\frac{A^2}{4gE_0^2(1-\rho^2)\sigma_R^2\sigma_I^2}\right) \times I_0\left(\frac{\sqrt{\left(\sigma_R^2-\sigma_I^2\right)^2+4\sigma_R^2\sigma_I^2\rho^2}}{4gE_0^2(1-\rho^2)\sigma_R^2\sigma_I^2}A^2\right), \tag{32}$$

with $I_0(x)$ denoting the modified Bessel function of the first kind. Equations (27) and (31) hold when both N and a are infinitely large, yet the density of scatterers fulfills $D = a/N \to 0$. In Appendix A we cover all the specific steps involved in the derivation of Eqs. (27) and (31).

Equation (31) is one of the main findings of our work, since it provides the amplitude distribution for unbiased random phases and any pair of distributions $\Omega(\phi)$ and $\nu(g)$, generalizing classic results [2,34,37] in the theory of speckle patterns. Let us analyze a few limiting cases of Eq. (31). In the regime of weak fluctuations in the number of scatterers [$\nu(g) = \delta(g-1)$], we get

$$\mathcal{P}_\beta(A) = \frac{A}{E_0^2\sigma_R\sigma_I\sqrt{1-\rho^2}} \exp\left(-\frac{A^2}{4E_0^2(1-\rho^2)\sigma_R^2\sigma_I^2}\right) \times I_0\left(\frac{\sqrt{\left(\sigma_R^2-\sigma_I^2\right)^2+4\sigma_R^2\sigma_I^2\rho^2}}{4E_0^2(1-\rho^2)\sigma_R^2\sigma_I^2}A^2\right). \tag{33}$$

Equation (33) depicts a novel amplitude distribution that applies to any phase distribution, as long as it satisfies the soft constraint $\langle e^{i\phi}\rangle_\phi = 0$. Since the argument of the Bessel function in the above equation is proportional to A^2, Eq. (33) is distinct from a Rice distribution [2]. The latter describes the statistics of the amplitude produced by a finite constant field plus a large number of small random fields with uniformly distributed phases [2]. When the phases are continuous random variables sampled from a uniform distribution in the interval $[0, 2\pi)$, Eqs. (28)–(30) result in

$$\sigma_R^2 = \sigma_I^2 = \tfrac{1}{2}, \quad \rho = 0 \tag{34}$$

and Eq. (33) simplifies to the well-known Rayleigh distribution

$$\mathcal{P}(A) = \frac{2A}{E_0^2}\exp\left(-\frac{A^2}{E_0^2}\right). \tag{35}$$

Thus, Eq. (33) essentially generalizes the Rayleigh distribution to nonuniform phase distributions. Figure 4 compares Eq. (33) with numerical histograms of the amplitude for two distinct distributions of unbiased phases in the regime of weak fluctuations in the number of scatterers. The numerical results are fully consistent with our analytic expression.

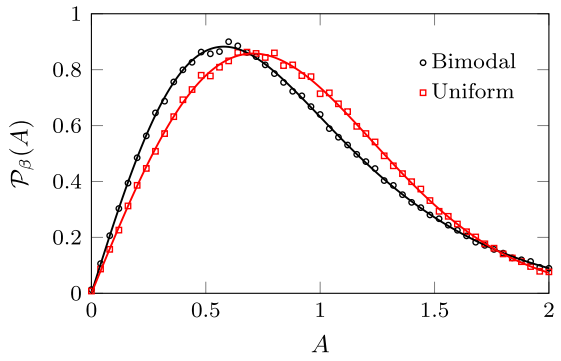

FIG. 4. Comparison between Eq. (33) (solid lines) and numerical histograms (symbols) for $\beta = \pi/2$ and weak fluctuations in the number of scatterers. The unbiased random phases follow a uniform distribution in the interval $[0, 2\pi)$ or they are sampled from the bimodal distribution of Eq. (11), with $q = 0.5$ and $\phi_0 = \pi/4$. The number of scatterers k follows a Poisson distribution with average $a = \sqrt{N}$. The numerical results are generated from 2×10^5 realizations of Eq. (3) with $N = 10^7$.

For random phases with a uniform distribution, we can substitute Eqs. (34) in Eq. (32), resulting in

$$\mathcal{P}(A) = \frac{2A}{E_0^2}\int_0^\infty \frac{dg\,\nu(g)}{g} e^{-A^2/gE_0^2}. \tag{36}$$

The distribution $\mathcal{P}(A)$ above is independent of the position β along the screen, regardless of the specific form of $\nu(g)$. When fluctuations in the number of scatterers are large ($\Delta_\nu > 0$), the universality associated with the central-limit theorem breaks down. As a result, the behavior of $\mathcal{P}(A)$ depends on the distribution $\nu(g)$. For example, when $\nu(g)$ follows a Γ distribution, we can substitute Eq. (16) into Eq. (36), integrate over the variable g, and arrive at the so-called K distribution [34,37]

$$\mathcal{P}(A) = \frac{4\mu^{(\mu+1)/2}}{E_0^{\mu+1}\Gamma(\mu)} A^\mu K_{\mu-1}\left(\frac{2\sqrt{\mu}}{E_0}A\right), \tag{37}$$

with $K_\mu(x)$ representing a modified Bessel function of the second kind.

Let us now turn our attention to the general equation (31). Depending on the specific form of $\nu(g)$, the integral in Eq. (31) has no analytic solution and one cannot derive a closed-form expression for $\mathcal{P}_\beta(A)$. However, when $\nu(g)$ is given by the Γ distribution (16), we show in Appendix B that, for any positive integer $\mu = n = 1, 2, \ldots$, the amplitude distribution can be calculated from the identity

$$\mathcal{P}_\beta(A) = \frac{A}{E_0^2\sigma_R\sigma_I\sqrt{1-\rho^2}} \frac{(-1)^{n-1}n^n}{(n-1)!} \left.\frac{\partial^{n-1}H(u)}{\partial u^{n-1}}\right|_{u=n}, \tag{38}$$

where $H(u)$ is given by

$$H(u) = 2I_0\left(\frac{A\,f(\omega)\sqrt{u}}{E_0\sigma_R\sigma_I\sqrt{1-\rho^2}}\right) K_0\left(\frac{A\,g(\omega)\sqrt{u}}{E_0\sigma_R\sigma_I\sqrt{1-\rho^2}}\right). \tag{39}$$

The functions $f(\omega)$ and $g(\omega)$ are defined as

$$f(\omega) = \begin{cases} \sin\omega & \text{if } 0 \leqslant \omega \leqslant \pi/4 \\ \cos\omega & \text{if } \pi/4 < \omega \leqslant \pi/2, \end{cases} \tag{40}$$

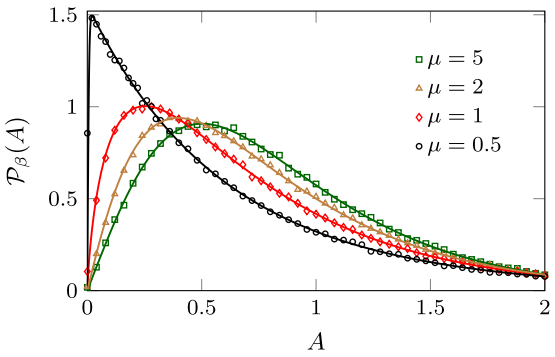

FIG. 5. Comparison between the theoretical results (solid lines) for the amplitude distribution and numerical results (symbols) for $\beta = \pi/2$ and unbiased random phases. The rescaled number of scatterers $\nu(g)$ follows a Γ distribution with variance $1/\mu$ [see Eq. (16)]. The phases are drawn from the bimodal distribution of Eq. (11), with $q = 0.5$ and $\phi_0 = \pi/4$. The numerical results (different symbols) are obtained from 2×10^5 realizations of the model with $N = 10^7$, where the number of scatterers is drawn from a negative binomial distribution with mean $a = \sqrt{N}$ [see Eq. (13)].

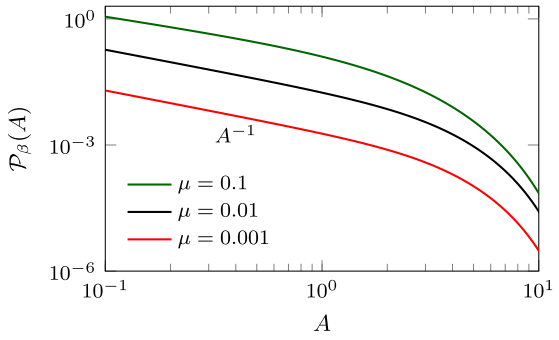

FIG. 6. Tails of the distribution of the amplitude for unbiased random phases and $\beta = \pi/2$. These results, obtained from Eq. (26), are shown in logarithmic scale. The rescaled number of scatterers follows a Γ distribution $\nu(g)$ with variance $1/\mu$ [see Eq. (16)]. The phases are drawn from the bimodal distribution of Eq. (11), with $q = 0.5$ and $\phi_0 = \pi/4$.

$$g(\omega) = \begin{cases} \cos\omega & \text{if } 0 \leqslant \omega \leqslant \pi/4 \\ \sin\omega & \text{if } \pi/4 < \omega \leqslant \pi/2, \end{cases} \tag{41}$$

where $\omega \in [0, \pi/2]$ is determined by $\Omega(\phi)$ as

$$\omega = \tfrac{1}{2}\sin^{-1}\left[\sqrt{\left(\sigma_R^2 - \sigma_I^2\right)^2 + 4\sigma_R^2\sigma_I^2\rho^2}\right]. \tag{42}$$

Equation (38) provides a practical way to obtain closed-form analytic expressions for $\mathcal{P}_\beta(A)$ when $\nu(g)$ is given by Eq. (16), with integer $\mu = n > 0$, and $\Omega(\phi)$ is an arbitrary distribution. Thus, Eq. (38) generalizes the K distribution of the amplitude, which is specific to uniform random phases, to any distribution of unbiased phases. The analytic expressions for $\mathcal{P}_\beta(A)$ when $\mu = 1$ and 2 are given by

$$\mathcal{P}_\beta(A) = \frac{2A}{E_0\gamma} I_0\left(\frac{Af(\omega)}{\gamma}\right) K_0\left(\frac{Ag(\omega)}{\gamma}\right) \tag{43}$$

and

$$\mathcal{P}_\beta(A) = \frac{2\sqrt{2}A^2}{E_0\gamma^2}\left[g(\omega) I_0\left(\frac{\sqrt{2}Af(\omega)}{\gamma}\right) K_1\left(\frac{\sqrt{2}Ag(\omega)}{\gamma}\right) - f(\omega) I_1\left(\frac{\sqrt{2}Af(\omega)}{\gamma}\right) K_0\left(\frac{\sqrt{2}Ag(\omega)}{\gamma}\right)\right], \tag{44}$$

respectively, with

$$\gamma = E_0\sigma_R\sigma_I\sqrt{1-\rho^2}. \tag{45}$$

In Appendix B we explain how to derive Eq. (38).

In Fig. 5 we compare our theoretical results with numerical histograms obtained from Eq. (3) in the regime of strong fluctuations in the number of scatterers. The solid curves for $\mu = 1$ and 2 are obtained from Eqs. (43) and (44), respectively, while the theoretical results for $\mu < 1$ are derived by numerically solving the integral in Eq. (31). The remarkable consistency between our analytic findings and numerical simulations confirms the exactness of our theory.

There are two distinctive features of $\mathcal{P}_\beta(A)$ when the phases are unbiased random variables and $\nu(g)$ follows Eq. (16). First, as shown in Fig. 5, the distribution $\mathcal{P}_\beta(A)$ goes to zero at $A = 0$ for any value of μ, in stark contrast to the behavior of $\mathcal{P}_\beta(A)$ for biased random phases [see Eq. (26)]. The complex field E is a sum of a large number of independent random variables. For unbiased phases, the fraction of samples or realizations with E exactly equal to zero decreases exponentially with N [48]. Therefore, in the limit $N \to \infty$, the fraction of samples with $A = 0$ goes to zero, regardless of the value of μ or the choice of the phase distribution. For biased phases, the statistics of E are controlled by the distribution of the rescaled number $g = k/a$ of scatterers. In the limit $a \to \infty$, samples that have a small number of scatterers in comparison to the mean a contribute with $E = 0$ to the statistics of E. Therefore, the fact that $\mathcal{P}_\beta(A \to 0)$ is nonzero for biased phases is a consequence of the finite fraction of samples with $g = k/a \to 0$.

The second interesting property concerns the right tail of the amplitude distribution. In Fig. 6 we plot $\mathcal{P}_\beta(A)$ for large A in the case of unbiased phases. For small μ and consequently strong fluctuations in the number of scatterers, the distribution $\mathcal{P}_\beta(A)$ exhibits once more a power-law tail up to a certain threshold, above which $\mathcal{P}_\beta(A)$ decays exponentially fast. Although this behavior is similar to the biased case, there is a key difference: The threshold value in Fig. 6 remains approximately independent of μ. For this reason, the probability of observing large fluctuations of the amplitude for unbiased phases is much smaller than for biased phases, for which the threshold value diverges as $\mu \to 0$ (see Fig. 3).

IV. CONCLUSION

In this work we have developed a comprehensive theory of speckle patterns based on the random-walk model. In this model, the resultant speckle field is the superposition of a stochastic number of partial waves, each with a random phase. The distribution of the number of scatterers and the distribution of phases are inputs of the model. By distinguishing between biased and unbiased random phases, we have derived general equations for the amplitude distribution of the

speckle field in the limit of an infinitely large mean number of scatterers. Once the phase distribution and the distribution of the number of scatterers are specified, our main findings, Eqs. (20) and (31), lead to closed-form analytic expressions that encompass a broad range of situations.

Two families of analytic results for unbiased random phases deserve special attention. First, when the number of scatterers is nonrandom, Eq. (31) yields a different form of the amplitude distribution which is the natural generalization of the Rayleigh law to nonuniform random phases. Second, when the number of scatterers is drawn from a negative binomial distribution with an integer scale parameter, Eq. (31) gives rise to generalizations of the K distribution to nonuniform phases. We have confirmed the exactness of these results by comparing them with numerical simulations for a bimodal phase distribution.

Interestingly, we have shown that the behavior of the amplitude distribution $\mathcal{P}_\beta(A)$ for large A is qualitatively distinct in the cases of biased and unbiased random phases. In both situations, $\mathcal{P}_\beta(A)$ displays a power-law decay up to a certain threshold, above which it decays exponentially fast (see Figs. 3 and 6). The difference appears in the threshold behavior as a function of the variance Δ_ν^2 of the number of scatterers. While for biased random phases this threshold increases as a function of Δ_ν^2, it remains approximately constant for unbiased random phases. This implies that a certain degree of phase coherence favors the generation of extremely large amplitudes, in line with previous works [26,27]. In this context, it would be interesting to quantify the impact of fluctuations of the number of scatterers in the formation of rogue intensity waves [26,49].

We expect that our analytic findings can be experimentally tested using a spatial light modulator (SLM). This device replicates the scattering from a rough surface through the phase modulation of an incident wave. When the SLM is illuminated by a laser beam, each pixel's diffraction on the SLM mask generates a partial wave with a specific phase. In principle, it is possible to imprint any sequence of random phases on the SLM [23,25,26], making it an ideal platform for testing our analytic predictions in the case of nonuniform phase distributions. However, an important drawback of this experimental setup is the limited number of pixels. Our main results for the amplitude distribution, Eqs. (20) and (31), are valid in the regime of low density of scatterers. This implies that both the sample size N (total number of pixels in a transversal direction) and the mean number of scatterers a (mean number of active pixels) are very large, but the density a/N goes to zero. In general, approaching this limit in SLM experiments may be a difficult task.

It would be interesting to compare our analytic findings for the amplitude distribution with results obtained from the numerical solutions of the Maxwell equations for large assemblies of scatterers distributed in space with a controllable density [50]. In this way, one could test whether the results obtained from the random-walk model serve as approximations to other relevant scenarios, such as in the study of speckle patterns formed by three-dimensional samples [8] or in the near-field regime. Another interesting research line is to investigate the connection between the parameters of our phenomenological random-walk model and the structural features characterizing models of interacting scattering particles, such as particle size and spatial correlations in the positions of the scatterers [51]. In this context, one expects that biased phase distributions are relevant to model the effects arising from spatial correlations.

To summarize, our analytic results expand the scope of the random-walk model of speckle patterns and open the perspective to systematically investigate the role of nonuniform phase distributions in a wide range of problems involving the linear superposition of random waves [11]. Our analytic techniques and results should be particularly useful to study nonisotropic random walks in finite dimensions [22,52,53].

ACKNOWLEDGMENTS

The authors thank R. R. B. Correia for useful comments. F.L.M. is grateful to Conselho Nacional de Desenvolvimento Científico e Tecnológico (CNPq-Brazil) for financial support.

APPENDIX A: DERIVATION OF THE AMPLITUDE DISTRIBUTION

In this Appendix we explain how to obtain the analytic results for the amplitude distribution. The first step is to calculate the characteristic function $\mathcal{G}_\beta(u, v)$ of the joint distribution $\mathcal{W}_\beta(E_R, E_I)$ of the real and imaginary parts of the speckle field $E(\beta) = E_R(\beta) + iE_I(\beta)$. The function $\mathcal{G}_\beta(u, v)$ is defined as

$$\mathcal{G}_\beta(u,v) = \left\langle \exp\left(-iuE_0\sum_{j=0}^{N-1} x_j \mathrm{Re}\mathcal{E}_j(\phi_j)\right) \times \exp\left(-ivE_0\sum_{j=0}^{N-1} x_j \mathrm{Im}\mathcal{E}_j(\phi_j)\right)\right\rangle_{\boldsymbol{x},\boldsymbol{\phi}}, \tag{A1}$$

with

$$\mathcal{E}_j(\phi_j) = e^{ij\beta/(N-1)+i\phi_j}. \tag{A2}$$

The symbols $\langle\cdots\rangle_{\boldsymbol{x}}$ and $\langle\cdots\rangle_{\boldsymbol{\phi}}$ denote the average over $x_0, \ldots, x_{N-1}$ and $\phi_0, \ldots, \phi_{N-1}$, respectively. The Fourier transform of $\mathcal{G}_\beta(u, v)$ yields $\mathcal{W}_\beta(E_R, E_I)$, namely,

$$\mathcal{W}_\beta(E_R, E_I) = \int_{-\infty}^{\infty} \frac{du\,dv}{4\pi^2} e^{iuE_R+ivE_I}\mathcal{G}_\beta(u, v). \tag{A3}$$

In order to calculate the average over $x_0, \ldots, x_{N-1}$ with the joint distribution (6), we need to factorize the conditional probability $P(\boldsymbol{x}|k)$, defined in Eq. (5), as a product over the index $j = 0, \ldots, N-1$ that identifies the scatterers. This is achieved by using the integral representation of the Kronecker δ,

$$\delta_{k,\sum_{j=0}^{N-1} x_j} = \int_0^{2\pi} \frac{dt}{2\pi} \exp\left[it\left(k - \sum_{j=0}^{N-1} x_j\right)\right], \tag{A4}$$

which allows us to rewrite $P(\boldsymbol{x}|k)$ as

$$P(\boldsymbol{x}|k) = \frac{1}{\mathcal{N}_k}\int_0^{2\pi} \frac{dt}{2\pi} e^{itk} \times \prod_{j=0}^{N-1} e^{-itx_j}\left[\frac{k}{N}\delta_{x_j,1} + \left(1 - \frac{k}{N}\right)\delta_{x_j,0}\right]. \tag{A5}$$

Combining the above expression with Eq. (6) and inserting the resulting form of $p(\boldsymbol{x})$ in Eq. (A1), we compute the average over $\boldsymbol{x}$ and obtain

$$\mathcal{G}_\beta(u,v) = \sum_{k=0}^{N} \frac{p_k}{\mathcal{N}_k} \int_0^{2\pi} \frac{dt}{2\pi} e^{itk} \times \exp\left[\sum_{j=0}^{N-1} \ln\left(1 + \frac{k}{N}[e^{-it} T_j(u,v) - 1]\right)\right], \tag{A6}$$

where we define

$$T_j(u,v) = \langle e^{-iuE_0 \mathrm{Re}\mathcal{E}_j(\phi) - ivE_0 \mathrm{Im}\mathcal{E}_j(\phi)} \rangle_\phi. \tag{A7}$$

The average $\langle f(\phi)\rangle_\phi$ of an arbitrary function $f(\phi)$ of a single phase ϕ is defined in Eq. (10).

In the limit $N \to \infty$, we can expand the logarithm in Eq. (A6) up to $O(1/N)$ and replace the sum over $j = 0, \ldots, N-1$ by an integral over $y \in [0,1]$,

$$\mathcal{G}_\beta(u,v) = \sum_{k=0}^{\infty} \frac{p_k}{\mathcal{N}_k^{(\infty)}} \int_0^{2\pi} \frac{dt}{2\pi} e^{-k+itk} \times \exp\left(k e^{-it} \int_0^1 dy \langle e^{-iu\,\mathrm{Re}\mathcal{E}_\phi(y) - iv\,\mathrm{Im}\mathcal{E}_\phi(y)} \rangle_\phi\right), \tag{A8}$$

where

$$\mathcal{E}_\phi(y) = E_0 e^{i\beta y + i\phi} \tag{A9}$$

and $\mathcal{N}_k^{(\infty)} = \frac{e^{-k}k^k}{k!}$ is the analytic expression for the normalization factor $\mathcal{N}_k$ when $N \to \infty$. By representing the second line of Eq. (A8) as a power series, we can integrate over t and arrive at the expression for the characteristic function in the limit $N \to \infty$,

$$\mathcal{G}_\beta(u,v) = \sum_{k=0}^{\infty} p_k e^{(k/a) Z_a(u,v)}, \tag{A10}$$

with

$$Z_a(u,v) = a \ln\left(\int_0^1 dy \langle e^{-iu\,\mathrm{Re}\mathcal{E}_\phi(y) - iv\,\mathrm{Im}\mathcal{E}_\phi(y)} \rangle_\phi\right). \tag{A11}$$

Equations (A10) and (A11) are valid as $N \to \infty$ while keeping a finite. The next step is to perform the limit $a \to \infty$ in the above equations. Since we first take the limit $N \to \infty$ followed by $a \to \infty$, the outcome of this order of limits is an analytic expression for the characteristic function $\mathcal{G}_\beta(E_R, E_I)$ in the low-density regime, i.e., when $D = \frac{a}{N} \to 0$. To perform the limit $a \to \infty$, we need to distinguish between biased and unbiased phases.

1. Biased phases

Let us consider phase distributions $\Omega(\phi)$ that fulfill the condition

$$\langle e^{i\phi} \rangle_\phi \neq 0. \tag{A12}$$

In this case, the random variable $\mathcal{E}_\phi(y)$ fluctuates around an average orientation in the complex plane. The most representative example of this family of distributions is when all phases are equal to a constant.

In order to perform the limit $\lim_{a\to\infty} Z_a(u,v)$ for this class of phase distributions, we have to rescale the amplitudes of the individual waves as $E_0 \to E_0/a$, and Eq. (A11) takes the form

$$Z_a(u,v) = a \ln\left[\int_0^1 dy \left\langle e^{-\frac{iu}{a}\mathrm{Re}\mathcal{E}_\phi(y) - \frac{iv}{a}\mathrm{Im}\mathcal{E}_\phi(y)} \right\rangle_\phi\right]. \tag{A13}$$

In the limit $a \to \infty$, $Z_a(u,v)$ converges to the expression

$$Z_\infty(u,v) = -iu \int_0^1 dy \langle \mathrm{Re}\mathcal{E}_\phi(y)\rangle_\phi - iv \int_0^1 dy \langle \mathrm{Im}\mathcal{E}_\phi(y)\rangle_\phi. \tag{A14}$$

Thus, by introducing the distribution $\nu(g)$ of the rescaled number of scatterers [Eq. (12)], the limit $a \to \infty$ of Eq. (A10) is given by

$$\mathcal{G}_\beta(u,v) = \int_0^\infty dg\, \nu(g) e^{g Z_\infty(u,v)}. \tag{A15}$$

From Eq. (A3) we thus find the corresponding expression for the joint distribution of the speckle field

$$\mathcal{W}_\beta(E_R, E_I) = \int_0^\infty dg\, \nu(g) \delta\left(E_R - g \int_0^1 dy \langle \mathrm{Re}\mathcal{E}_\phi(y)\rangle_\phi\right) \times \delta\left(E_I - g \int_0^1 dy \langle \mathrm{Im}\mathcal{E}_\phi(y)\rangle_\phi\right). \tag{A16}$$

Therefore, the fluctuations of the real and the imaginary parts of $E(\beta)$ are solely determined by $\nu(g)$, with the amplitude $A(\beta)$ relating to g as

$$A(\beta) \underline{\underline{d}}\, g |E_*(\beta)|, \tag{A17}$$

where

$$E_*(\beta) = \int_0^1 dy \langle \mathrm{Re}\mathcal{E}_\phi(y)\rangle_\phi + i \int_0^1 dy \langle \mathrm{Im}\mathcal{E}_\phi(y)\rangle_\phi. \tag{A18}$$

The symbol $\underline{\underline{d}}$ in Eq. (A17) means that both sides of the equation are equal in a distributional sense. Equation (A17) immediately implies that the amplitude distribution $\mathcal{P}_\beta(A)$ is determined by $\nu(g)$ according to Eq. (20).

2. Unbiased phases

Here we consider phase distributions $\Omega(\phi)$ that satisfy the constraint

$$\langle e^{i\phi} \rangle_\phi = 0. \tag{A19}$$

In this case, the average of the complex random variable $\mathcal{E}_\phi(y)$ is zero. The most representative example of this class of distributions is when the phases are continuous random variables drawn from a uniform distribution in $[0, 2\pi)$.

For phase distributions that fulfill Eq. (A19), we rescale the amplitude E_0 as $E_0 \to E_0/\sqrt{a}$ and Eq. (A11) assumes the form

$$Z_a(u,v) = a \ln\left[\int_0^1 dy \left\langle e^{-\frac{iu}{\sqrt{a}}\mathrm{Re}\mathcal{E}_\phi(y) - \frac{iv}{\sqrt{a}}\mathrm{Im}\mathcal{E}_\phi(y)} \right\rangle_\phi\right]. \tag{A20}$$

By expanding the right-hand side of the above equation in powers of $1/\sqrt{a}$, we can show that $\lim_{a\to\infty} Z_a(u,v)$ is given

by the quadratic form

$$Z_\infty(u,v) = -\tfrac{1}{2}E_0^2\sigma_R^2u^2 - \tfrac{1}{2}E_0^2\sigma_I^2v^2 - uvE_0^2\sigma_R\sigma_I\rho, \quad \text{(A21)}$$

where σ_R^2, σ_I^2, and ρ are defined by Eqs. (28)–(30). Substituting this result in Eq. (A10) and taking the limit $a \to \infty$, we obtain the characteristic function

$$\mathcal{G}_\beta(u,v) = \int_0^\infty dg\, \nu(g) e^{gZ_\infty(u,v)}. \quad \text{(A22)}$$

Inserting Eq. (A22) in Eq. (A3) and calculating the Gaussian integrals over u and v, we find the joint distribution of the complex field

$$\mathcal{W}_\beta(E_R,E_I) = \frac{1}{2\pi E_0^2\sigma_R\sigma_I\sqrt{1-\rho^2}}\int_0^\infty \frac{dg}{g}\nu(g) \times \exp\left[-\frac{1}{2gE_0^2(1-\rho^2)} \times\left(\frac{E_R^2}{\sigma_R^2}+\frac{E_I^2}{\sigma_I^2}-\frac{2\rho E_RE_I}{\sigma_R\sigma_I}\right)\right]. \quad \text{(A23)}$$

When the distribution of the number of scatterers is such that $\nu(g) = \delta(g-1)$, $\mathcal{W}_\beta(E_R,E_I)$ follows a bivariate Gaussian distribution, which is a consequence of the central-limit theorem. When the variance of $\nu(g)$ is finite, the central-limit theorem fails and $\mathcal{W}_\beta(E_R,E_I)$ depends on the form of $\nu(g)$.

Equation (A23) enables us to obtain the amplitude distribution for any $\nu(g)$. Let $G_\beta(S)$ be the characteristic function of the probability density $P_\beta(I)$ of the intensity $I \underline{=} E_R^2 + E_I^2$, namely,

$$G_\beta(S) = \int_{-\infty}^\infty dE_R dE_I \mathcal{W}_\beta(E_R,E_I) e^{-iS(E_R^2+E_I^2)}. \quad \text{(A24)}$$

The distribution $P_\beta(I)$ follows from the Fourier transform

$$P_\beta(I) = \int_{-\infty}^\infty \frac{dS}{2\pi} e^{iSI} G_\beta(S). \quad \text{(A25)}$$

Substituting Eq. (A23) into Eq. (A24) and performing the Gaussian integrals over E_R and E_I, we arrive at the expression

$$G_\beta(S) = \frac{1}{E_0^2\sigma_R\sigma_I\sqrt{1-\rho^2}}\int_0^\infty \frac{dg}{g}\nu(g) \times\left[\left(2iS+\frac{1}{gE_0^2(1-\rho^2)\sigma_R^2}\right) \times\left(2iS+\frac{1}{gE_0^2(1-\rho^2)\sigma_I^2}\right) -\frac{\rho^2}{g^2E_0^4(1-\rho^2)^2\sigma_R^2\sigma_I^2}\right]^{-1/2}. \quad \text{(A26)}$$

The final act is the calculation of the Fourier transform in Eq. (A25). Combining Eqs. (A26) and (A25), we can rewrite $P_\beta(I)$ as

$$P_\beta(I) = \frac{1}{4\pi E_0^2\sigma_R\sigma_I\sqrt{1-\rho^2}}\int_0^\infty \frac{dg}{g}\nu(g) \times\int_{-\infty}^\infty \frac{dS\, e^{-iSI}}{(r_+ - iS)^{\frac{1}{2}}(r_- - iS)^{1/2}}, \quad \text{(A27)}$$

where we have defined

$$r_\pm = \frac{1}{4gE_0^2(1-\rho^2)\sigma_R^2\sigma_I^2} \times\left[\sigma_R^2+\sigma_I^2 \pm \sqrt{\left(\sigma_R^2-\sigma_I^2\right)^2+4\sigma_R^2\sigma_I^2\rho^2}\right]. \quad \text{(A28)}$$

Following [54], we integrate over the variable S in Eq. (A27), obtaining

$$P_\beta(I) = \frac{1}{2E_0^2\sigma_R\sigma_I\sqrt{1-\rho^2}}\int_0^\infty \frac{dg\,\nu(g)}{g} e^{-I/4gE_0^2(1-\rho^2)\sigma_R^2\sigma_I^2} \times I_0\left(\frac{\sqrt{\left(\sigma_R^2-\sigma_I^2\right)^2+4\sigma_R^2\sigma_I^2\rho^2}}{4gE_0^2(1-\rho^2)\sigma_R^2\sigma_I^2}I\right), \quad \text{(A29)}$$

where $I_0(x)$ is a modified Bessel function of the first kind. The above expression gives the distribution of the intensity $I \underline{d} A^2$. We find Eq. (31) for the amplitude distribution $\mathcal{P}_\beta(A)$ by making a simple change of variables.

APPENDIX B: AMPLITUDE DISTRIBUTION FOR INTEGER μ

Here we explain how to obtain Eq. (38), which leads to analytic expressions for $\mathcal{P}_\beta(A)$ when $\nu(g)$ is given by the Γ distribution of Eq. (16) with integer μ. Substituting Eq. (16) into Eq. (31) and setting $\mu = n \in \mathbb{Z}^+$, we get the general expression

$$\mathcal{P}_\beta(A) = \frac{A}{E_0^2\sigma_R\sigma_I\sqrt{1-\rho^2}}\frac{n^n}{2^{n-1}(n-1)!}\int_0^\infty dg\, g^{n-2}e^{-ng/2} \times\exp\left(-\frac{A^2}{2E_0^2(1-\rho^2)\sigma_R^2\sigma_I^2 g}\right) \times I_0\left(\frac{\sqrt{\left(\sigma_R^2-\sigma_I^2\right)^2+4\sigma_R^2\sigma_I^2\rho^2}\,A^2}{2E_0^2(1-\rho^2)\sigma_R^2\sigma_I^2 g}\right). \quad \text{(B1)}$$

Now we introduce an alternative parametrization of the constants that depend on σ_R, σ_I, and ρ. Let us define the positive variables

$$X = \frac{A}{E_0\sigma_R\sigma_I\sqrt{1-\rho^2}}\cos(\omega),$$
$$Y = \frac{A}{E_0\sigma_R\sigma_I\sqrt{1-\rho^2}}\sin(\omega),$$

where the polar angle $\omega \in [0, \pi/2]$ is given by Eq. (42). We can check that X and Y fulfill

$$X^2 + Y^2 = \frac{A^2}{E_0^2(1-\rho^2)\sigma_R^2\sigma_I^2}$$

and

$$XY = \frac{\sqrt{(\sigma_R^2 - \sigma_I^2)^2 + 4\sigma_R^2\sigma_I^2\rho^2}\,A^2}{2E_0^2(1-\rho^2)\sigma_R^2\sigma_I^2},$$

which allows us to rewrite Eq. (B1) as

$$\mathcal{P}_\beta(A) = \frac{A}{E_0^2\sigma_R\sigma_I\sqrt{1-\rho^2}}\frac{n^n}{2^{n-1}(n-1)!}\int_0^\infty dg\, g^{n-2}e^{-ng/2} \times \exp\left(-\frac{(X^2+Y^2)}{2g}\right)I_0\left(\frac{XY}{g}\right). \tag{B2}$$

Our aim is to find a convenient way to calculate the integral over g in Eq. (B2). This integral can be seen as the $(n-2)$th integer moment of the variable g, whose unnormalized distribution is a product of an exponential and a modified Bessel function of the first kind. The idea is to express higher-order moments ($n > 1$) in terms of derivatives of the lowest-order moment ($n = 1$). This is a standard technique in statistical physics, which is implemented here by defining the function

$$H_n(u) = \int_0^\infty dg\, g^{n-2}\exp\left(-\frac{ug}{2} - \frac{(X^2+Y^2)}{2g}\right)I_0\left(\frac{XY}{g}\right) \tag{B3}$$

of the variable $u \in \mathbb{R}^+$. The integral appearing in Eq. (B2) is recovered by calculating the function $H_n(u)$ at $u = n$. Thus, by defining $H(u) := H_1(u)$ and noting that

$$\frac{\partial^{n-1}H(u)}{\partial u^{n-1}} = \left(-\frac{1}{2}\right)^{n-1}H_n(u) \quad (n > 1), \tag{B4}$$

we rewrite Eq. (B2) as

$$\mathcal{P}_\beta(A) = \frac{A}{E_0^2\sigma_R\sigma_I\sqrt{1-\rho^2}}\frac{(-1)^{n-1}n^n}{(n-1)!}\left.\frac{\partial^{n-1}H(u)}{\partial u^{n-1}}\right|_{u=n}. \tag{B5}$$

The above equation becomes a powerful identity to compute $\mathcal{P}_\beta(A)$ only if we are able to solve the integral

$$H(u) = \int_0^\infty \frac{dg}{g}\exp\left(-\frac{ug}{2} - \frac{(X^2+Y^2)}{2g}\right)I_0\left(\frac{XY}{g}\right). \tag{B6}$$

Fortunately, it is possible to calculate the above integral using [55]. The result is given by Eq. (39), which demonstrates Eq. (38).

[1] A. Ishimaru, *Wave Propagation and Scattering in Random Media* (Wiley, New York, 1999).

[2] J. W. Goodman, Some fundamental properties of speckle, J. Opt. Soc. Am. **66**, 1145 (1976).

[3] J. W. Goodman, *Speckle Phenomena in Optics* (Viva Books, New Delhi, 2008).

[4] R. Carminati, Hidden statistics in speckle patterns, Photoniques **110**, 32 (2021).

[5] A. Dogariu and R. Carminati, Electromagnetic field correlations in three-dimensional speckles, Phys. Rep. **559**, 1 (2015), electromagnetic field correlations in three-dimensional speckles.

[6] S. M. Cohen, D. Eliyahu, I. Freund, and M. Kaveh, Vector statistics of multiply scattered waves in random systems, Phys. Rev. A **43**, 5748 (1991).

[7] I. Freund, Optical vortices in gaussian random wave fields: Statistical probability densities, J. Opt. Soc. Am. A **11**, 1644 (1994).

[8] S. E. Skipetrov and I. M. Sokolov, Intensity of waves inside a strongly disordered medium, Phys. Rev. Lett. **123**, 233903 (2019).

[9] M. Leonetti, L. Pattelli, S. De Panfilis, D. S Wiersma, and G. Ruocco, Spatial coherence of light inside three-dimensional media, Nat. Commun. **12**, 4199 (2021).

[10] F. Ott and A. Kienle, Lambertian illumination of dielectric scattering media with monochromatic light, Phys. Rev. A **105**, 033528 (2022).

[11] J. M. Dudley, G. Genty, A. Mussot, A. Chabchoub, and F. Dias, Rogue waves and analogies in optics and oceanography, Nat. Rev. Phys. **1**, 675 (2019).

[12] M. Draijer, E. Hondebrink, T. van Leeuwen, and W. Steenbergen, Review of laser speckle contrast techniques for visualizing tissue perfusion, Lasers Med. Sci. **24**, 639 (2009).

[13] A. Gatti, M. Bache, D. Magatti, E. Brambilla, F. Ferri, and L. A. Lugiato, Coherent imaging with pseudo-thermal incoherent light, J. Mod. Opt. **53**, 739 (2006).

[14] J. Shin, B. T. Bosworth, and M. A. Foster, Single-pixel imaging using compressed sensing and wavelength-dependent scattering, Opt. Lett. **41**, 886 (2016).

[15] Z. Ye, D. Sheng, Z. Hao, H.-Bo. Wang, J. Xiong, X. Wang, and W. Jin, Pseudo-thermal ghost imaging with learned wavelength conversion, Appl. Phys. Lett. **117**, 091103 (2020).

[16] E. Valent and Y. Silberberg, Scatterer recognition via analysis of speckle patterns, Optica **5**, 204 (2018).

[17] V. M. Castilho, W. F. Balthazar, L. da Silva, T. J. P. Penna, and J. A. O. Huguenin, Machine learning classification of speckle patterns for roughness measurements, Phys. Lett. A **468**, 128736 (2023).

[18] J. M. Senior, *Optical Fiber Communications: Principles and Practice* (Pearson, London, 2009).

[19] G. R. Osche, *Optical Detection Theory for Laser Applications* (Wiley, New York, 2002).

[20] A. D. Mirlin, Statistics of energy levels and eigenfunctions in disordered systems, Phys. Rep. **326**, 259 (2000).

[21] J. Wang and A. Genack, Transport through modes in random media, Nature (London) **471**, 345 (2011).

[22] E. Jakeman and R. J. A. Tough, Generalized K distribution: A statistical model for weak scattering, J. Opt. Soc. Am. A **4**, 1764 (1987).

[23] Y. Bromberg and H. Cao, Generating non-Rayleigh speckles with tailored intensity statistics, Phys. Rev. Lett. **112**, 213904 (2014).

[24] N. Bender, H. Yilmaz, Y. Bromberg, and H. Cao, Customizing speckle intensity statistics, Optica **5**, 595 (2018).
[25] N. Bender, H. Yilmaz, Y. Bromberg, and H. Cao, Creating and controlling complex light, APL Photon. **4**, 110806 (2019).
[26] C. Bonatto, S. D. Prado, F. L. Metz, J. R. Schoffen, R. R. B. Correia, and J. M. Hickmann, Super rogue wave generation in the linear regime, Phys. Rev. E **102**, 052219 (2020).
[27] R. da Silva and S. D. Prado, A simple study of the correlation effects in the superposition of waves of electric fields: The emergence of extreme events, Phys. Lett. A **384**, 126231 (2020).
[28] P. N. Pusey, D. W. Schaefer, and D. E. Koppel, Single-interval statistics of light scattered by identical independent scatterers, J. Phys. A: Math. Nucl. Gen. **7**, 530 (1974).
[29] I. A. Popov, N. V. Sidorovsky, and L. M. Veselov, Experimental study of intensity probability density function in the speckle pattern formed by a small number of scatterers, Opt. Commun. **97**, 304 (1993).
[30] T. R. Watts, K. I. Hopcraft, and T. R. Faulkner, Single measurements on probability density functions and their use in non-Gaussian light scattering, J. Phys. A: Math. Gen. **29**, 7501 (1996).
[31] B. Shapiro, Large intensity fluctuations for wave propagation in random media, Phys. Rev. Lett. **57**, 2168 (1986).
[32] R. Dashen, Path integrals for waves in random media, J. Math. Phys. **20**, 894 (1979).
[33] A. D. Mirlin, R. Pnini, and B. Shapiro, Intensity distribution for waves in disordered media: Deviations from Rayleigh statistics, Phys. Rev. E **57**, R6285 (1998).
[34] E. Jakeman and P. N. Pusey, Significance of K distributions in scattering experiments, Phys. Rev. Lett. **40**, 546 (1978).
[35] R. L. Phillips and L. C. Andrews, Measured statistics of laser-light scattering in atmospheric turbulence, J. Opt. Soc. Am. **71**, 1440 (1981).
[36] E. Jakeman and R. J. A. Tough, Non-Gaussian models for the statistics of scattered waves, Adv. Phys. **37**, 471 (1988).
[37] E. Jakeman, On the statistics of K-distributed noise, J. Phys. A: Math. Gen. **13**, 31 (1980).
[38] M. Kazmierczak, T. Keyes, and T. Ohtsuki, Determination of the number of scatterers in a finite volume by the statistical analysis of scattered light intensity, Phys. Rev. B **39**, 1315 (1989).
[39] A. Apostol and A. Dogariu, Spatial correlations in the near field of random media, Phys. Rev. Lett. **91**, 093901 (2003).
[40] A. Apostol and A. Dogariu, Non-Gaussian statistics of optical near-fields, Phys. Rev. E **72**, 025602(R) (2005).
[41] A. Apostol, D. Haefner, and A. Dogariu, Near-field characterization of effective optical interfaces, Phys. Rev. E **74**, 066603 (2006).
[42] R. R. Naraghi, S. Sukhov, and A. Dogariu, Disorder fingerprint: Intensity distributions in the near field of random media, Phys. Rev. B **94**, 174205 (2016).
[43] R. Barakat, Weak-scatterer generalization of the K-density function with application to laser scattering in atmospheric turbulence, J. Opt. Soc. Am. A **3**, 401 (1986).
[44] F. T. Arecchi, U. Bortolozzo, A. Montina, and S. Residori, Granularity and inhomogeneity are the joint generators of optical rogue waves, Phys. Rev. Lett. **106**, 153901 (2011).
[45] A. Mathis, L. Froehly, S. Toenger, F. Dias, G. Genty, and J. M. Dudley, Caustics and rogue waves in an optical sea, Sci. Rep. **5**, 12822 (2015).
[46] A. Safari, R. Fickler, M. J. Padgett, and R. W. Boyd, Generation of caustics and rogue waves from nonlinear instability, Phys. Rev. Lett. **119**, 203901 (2017).
[47] M. Tlidi and M. Taki, Rogue waves in nonlinear optics, Adv. Opt. Photon. **14**, 87 (2022).
[48] H. Touchette, The large deviation approach to statistical mechanics, Phys. Rep. **478**, 1 (2009).
[49] A. R. C. Buarque, W. S. Dias, G. M. A. Almeida, M. L. Lyra, and F. A. B. F. de Moura, Rogue waves in quantum lattices with correlated disorder, Phys. Rev. A **107**, 012425 (2023).
[50] L. Pattelli, A. Egel, U. Lemmer, and D. S. Wiersma, Role of packing density and spatial correlations in strongly scattering 3D systems, Optica **5**, 1037 (2018).
[51] M. Almasian, T. G. van Leeuwen, and D. J. Faber, Oct amplitude and speckle statistics of discrete random media, Sci. Rep. **7**, 14873 (2017).
[52] B. C. Barber, The non-isotropic two-dimensional random walk, Waves Random Media **3**, 243 (1993).
[53] A. De Gregorio, On random flights with non-uniformly distributed directions, J. Stat. Phys. **147**, 382 (2012).
[54] I. S. Gradshteyn and I. M. Ryzhik, in *Table of Integrals, Series, and Products*, 6th ed., edited by A. Jeffrey (Elsevier, Amsterdam, 2000), p. 345.
[55] I. S. Gradshteyn and I. M. Ryzhik, in *Table of Integrals, Series, and Products* (Ref. [54]), p. 705.